CBPF-NF-005/98

Cold fission description with constant and varying mass asymmetries

S.B. Duarte[1], *O. Rodríguez*[1†], *O.A.P Tavares*[1], *M. Gonçalves*[2*], *F. García*[3†] *and F. Guzmán*[3†]

[1]Centro Brasileiro de Pesquisas Físicas – CBPF/CNPq,
R. Dr. Xavier Sigaud, 150,
22290-180 Rio de Janeiro-RJ, Brazil

[2]Instituto de Radioproteção e Dosimetria-IRD/CNEN,
Av. Salvador Allende s/n,
22780-160 Rio de Janeiro-RJ, Brazil

[3]Instituto de Física, Universidade de São Paulo,
Caixa Postal 66318,
05315-970 São Paulo, Brazil

Abstract

Different descriptions for varying the mass asymmetry in the fragmentation process are used to calculate the cold fission barrier penetrability. The relevance of the appropriate choice for both the description of the pre-scission phase and inertia coefficient to unify alpha decay, cluster radioactivity, and spontaneous cold fission processes in the same theoretical framework is explicitly shown. We calculate the half-life of all possible partition modes of nuclei of $A > 200$ following the most recent Mass Table by Audi and Wapstra. It is shown that if one uses the description in which the mass asymmetry is maintained constant during the fragmentation process, the experimental half-life-values and mass yield of ^{234}U cold fission are satisfactorily reproduced.

PACS number(s): 23.70.+j, 23.90+Wg, 25.85.Ca

---

*Author to whom correspondence should be sent: telo@ird.gov.br

†Permanent address: Instituto Superior de Ciências y Tecnologia Nucleares, Av. Salvador Allende y Luaces, Apartado Postal 6163, La Habana, Cuba

I. INTRODUCTION

Theoretical predictions for new nuclear radioactive decay modes have been made in a recent past [1–3] in the framework of the fragmentation theory [4,5], based on the two-center shell model. The idea has been constrained to the cold rearrangements of a large number of nucleons in the ground state of the parent nucleus. The existence of a new valley in the potential energy surface for heavy cluster emission in which one of the emitted fragments is close to the double magic shell has been pointed out by Săndulescu and Greiner [1]. Theoretical attempts to understand cluster radioactivity assume either a strongly asymmetric fission process or a clustering pre-formation followed by fragment emission. In these treatments the emission of light clusters such as ^{14}C has been interpreted in terms of 'cluster decay', while for the heavier fragment emission modes (^{24}Ne, ^{30}Mg, ^{34}Si, and ^{48}Ca) the 'fission approach' has been used [6]. Although the similarity between alpha-particle decay and cold fission process was recognized in the early stages of the fission theory by Borh [7], the theories employed to treat these two phenomena have been developed by using different approaches. As concerning alpha decay, microscopic methods of nuclear reactions have been largely employed. On the other hand, the fission theory has been treated for many years in terms of phenomenological liquid drop models, which have been improved by incorporating the microscopic shell correction method [8].

Nuclear cold fission process associated with cluster radioactivity has been explored intensively in the last five years or so from the experimental and theoretical point of views [9–30]. The occurrence of cold fission processes for which no neutron emission takes place, and the total kinetic energy of the final fragments practically exhausts the Q-value, are related to shell effects on the barrier penetrability factor.

Very recently, after the observation of the cold fission process in ^{236}U* (from thermal-neutron-induced fission of ^{235}U [24]) and ^{252}Cf [10,25,26] nuclei, other new cases for cold fission have been detected experimentally in ^{230}Th [27], ^{233,234}U [27,28], ^{236,238,240,242,244}Pu

[27,29,30], and ^{248}Cm [11] isotopes. At the same time, new theoretical approaches have been proposed [12–17] in order to describe alpha radioactivity, cluster emission and cold fission reactions in a unified image.

An effective model to describe cluster radioactivity and alpha decay processes in terms of an analytical Coulomb potential and nuclear interaction during the pre-scission phase has been recently proposed by Gonçalves and Duarte [18,19]. This model successfully reproduces all observed half-life data of cluster radioactivity by using only one adjustable parameter, the nuclear radius constant, r_0, appearing in the nuclear radius definition, $R = r_0 A^{1/3}$.

In the present work we extend our model to include also cold fission processes. We discuss the role of inertia coefficients in relation to half-lives and product yields. An extensive calculation for all possible partition modes of nuclei following the available mass data by Audi and Wapstra [31] with a positive Q-value and parent nucleus mass number $A > 200$ is performed. The results are strongly dependent on the prescription to describe the changing of the mass asymmetry parameter during the fragmentation process. We would like to call attention to the fact that in spite of using an schematic parameterization to the geometric shape during the pre-scission phase, we are able to reproduce the ^{234}U cold fission half-life, as well as the ^{234}U mass yield distribution satisfactorily. It is important to remark that in the present stage we are not taking explicitly into account the deformation of fragments. The results of cold fission calculation with different descriptions for varying the mass asymmetry in the fragmentation process allows to choose the more appropriate description for the effective one-dimensional approach.

In Section II we summarize the fundamentals of the model concerning shape parameterization, constraint relationships, and the coordinates chosen to describe the configuration of the pre-scission dinuclear regime. In Section III we extend our previous model to cold fission processes, and in the last Section we conclude with final remarks.

II. THE PRE-SCISSION PHASE DESCRIPTION

The geometric shape parameterization during the pre-scission phase of the fissioning nuclear system is the same adopted in previous works [18–20,32–35]. The dinuclear phase is parameterized as two intersecting spheres, and two different descriptions for the pre-scission phase are considered, namely, the Varying Mass Asymmetry Shape (VMAS) and the Constant Mass Asymmetry Shape (CMAS) (called, respectively, as cluster-like and more compact shape in [36]). In the first description, the masses of the nascent fragments are changing with the increasing of the distance between the geometric center of fragments. The mass asymmetry parameter, $\eta = (m_1 - m_2)/(m_1 + m_2)$, varies from unit to the final mass asymmetry of the products. The second description imposes a constant value of the mass asymmetry defined as the mass asymmetry of the final products. There is no change in mass of the nascent fragments during the whole pre-scission phase in the second description. In both cases, the nascent fragments configuration is determined by the specification of four independent collective coordinates: the radii R_1 and R_2 of the fragments, the distance between the centers of the fragments, ζ, and the distance from the center of heavier nucleus to the intersecting plane of the spherical fragments, ξ (see Fig. 1 in Ref. [18]).

To calculate Gamow's penetrability factor [37] for the one-dimensional problem, three of these collective coordinates should be eliminated preserving the shape and the incompressibility of the nuclear matter constraint relationships. Thus, we imposed that the whole volume of the dinuclear system is constant, i.e.,

$$2(R_1^3 + R_2^3) + 3\left[R_1^2(\zeta - \xi) + R_2^2\xi\right] - \left[(\zeta - \xi)^3 + \xi^3\right] - 4R_0^3 \;=\; 0 \;\;, \tag{1}$$

where R_0 is the radius of the parent nucleus.

In order to keep the circular shape for the neck connecting the nascent fragments, the following geometric relationship is introduced

$$R_1^2 - R_2^2 - (\zeta - \xi)^2 + \xi^2 \;=\; 0 \;\;. \tag{2}$$

Finally, an additional constraint relationship will distinguish the two different descriptions (VMAS or CMAS). To characterize the VMAS description we regarded the radius of the lighter fragment as constant, i.e.,

$$R_1 - \bar{R}_1 \;=\; 0\;, \tag{3}$$

where $\bar{R}_1$ is the final radius of the light fragment.

In the CMAS description the volume of fragments is constant, and in terms of the lighter fragment the volume conservation is given by

$$2R_1^3 + 3R_1^2(\zeta - \xi) - (\zeta - \xi)^3 - 4\bar{R}_1^3 \;=\; 0\;. \tag{4}$$

Once the system is reduced to the one-dimensional case, the barrier penetrability factor can be calculated in terms of the geometric separation between the centers of the fragments, ζ, by

$$\mathcal{P} \;=\; \exp\left\{-\frac{2}{\hbar}\int_{\zeta_0}^{\zeta_C}\sqrt{2\mu\,(V-Q)}\mathrm{d}\zeta\right\}\quad, \tag{5}$$

where ζ_0 and ζ_C are, respectively, the inner and outer turning points, and Q stands for the kinetic energy available in the decay. The total potential energy, V, which appears in Eq. (5), is determined by using an analytical solution of Poisson's equation for the Coulomb part, and an effective surface potential of a liquid drop for the nuclear component. The experimental Q-value is introduced into the calculation to determine the outer turning point $\zeta = Z_1 Z_2 e^2/Q$, and also to define the effective surface potential of the drop, by establishing that the difference between the initial and final asymptotic configurations of the fissioning system reproduce the experimental Q-value (see details in Ref. [18]). The potential barrier is illustrated in Fig. 1 as a function of the ζ coordinate for three modes of decay of ^{234}U parent nucleus. The potentials in the VMAS and the CMAS descriptions for the same nuclear geometric parameters are explicitly shown. We remark that no significant differences between the two curves for the decay processes in ^{234}U isotope are observed.

As usual, the decay rate is calculated by

$$\lambda \;=\; \lambda_0 \, \mathcal{P} \quad , \tag{6}$$

where $\lambda_0 = 10^{22}\mathrm{s}^{-1}$ is the frequency of assaults on the barrier.

To determine Gamow's penetrability factor we need to know the inertia coefficient, μ (Eq. (5)). Werner-Wheeler's approximation [36] for the velocity field of the nuclear flow to define the inertia tensor coefficient has been largely used in the literature [18,32]. In this approach the velocity field is obtained from the solution of the continuity equation, by using the incompressibility and irrotationality of the nuclear flow. After reduction to the one-dimensional relative motion of the separating parts, only one component of the tensor becomes relevant. The expression for Werner-Wheeler's inertia coefficient is given by

$$\frac{1}{2}\int \rho \vec{v}^{\,2} \mathrm{d}r \;=\; \frac{1}{2}\mu_{WW}\dot{\zeta}^{\,2} \quad , \tag{7}$$

where ρ is the mass density for the system, and $\dot{\zeta}$ is the relative velocity of the geometric center of the fragments. We can determine Werner-Wheeler's inertia coefficient for the two parameterizations, namely, μ_{WW}^{VMAS} and μ_{WW}^{CMAS} [18,32].

An alternative proposal for calculating the inertia coefficient has been recently applied in one-dimensional penetrability calculations [19]. By means of a straightforward calculation regarding the constraints above (Eqs. (1–3)), the expression for the effective inertia coefficient reads

$$\mu_{\mathrm{eff}} \;=\; \mu\alpha^2 \quad , \tag{8}$$

where $\mu = m_1 m_2/(m_1+m_2)$ is the reduced mass of the nascent fragments. For the VMAS description we have

$$\alpha^{\mathrm{VMAS}} \;=\; 1 - \frac{2}{\zeta(R_2-\xi)}\left[(\zeta-\xi)(\bar{z}_1+\bar{z}_2) + \bar{z}_1^{\,2} - \bar{z}_2^{\,2}\right] \quad , \tag{9}$$

where the variable $\bar{z}_i$ is given by

$$\bar{z}_1 = \frac{\pi}{4}\left[R_1^2 - (\zeta-\xi)^2\right]^2 / v_1 \tag{10}$$

$$\bar{z}_2 = \frac{\pi}{4}\left[R_2^2 - \xi^2\right] / v_2 \ , \tag{11}$$

in which $v_1 = \frac{\pi}{3}\left[2R_1^3 + 3R_1^2(\zeta-\xi) - (\zeta-\xi)^3\right]$ and $v_2 = \frac{\pi}{3}\left[2R_2^3 + 3R_2^2\xi - \xi^3\right]$ are the volumes of each spherical segment.

For the CMAS description, where the mass of the fragments does not vary during the pre-scission phase, we have

$$\begin{aligned}\alpha^{\rm CMAS} = 1 &+ \frac{1}{v_1}\left[R_1^2 - (\zeta-\xi)^2\right]\left[R_1\frac{dR_1}{d\zeta} - (\zeta-\xi)\left(1 - \frac{d\xi}{d\zeta}\right)\right] \\ &+ \frac{1}{v_2}\left(R_2^2 - \xi^2\right)\left(R_2\frac{dR_2}{d\zeta} - \xi\frac{d\xi}{d\zeta}\right),\end{aligned} \tag{12}$$

where

$$\frac{d\xi}{d\zeta} = -\gamma\frac{dR_2}{d\zeta} \ , \tag{13}$$

$$\frac{dR_1}{d\zeta} = \frac{1}{R_1}\left[(\zeta-\xi) + (R_2 + \gamma\zeta)\frac{dR_2}{d\zeta}\right] \ , \tag{14}$$

$$\frac{dR_2}{d\zeta} = -\frac{(\zeta-\xi)(6R_1 + 4\zeta - 4\xi) + R_1(5R_1 + 3\zeta - 3\xi)}{(R_2 + \gamma\zeta)(6R_1 + 4\zeta - 4\xi) + \gamma R_1(5R_1 + 3\zeta - 3\xi)} \ , \tag{15}$$

and

$$\gamma = \left(\frac{6R_2 + 4\xi}{5R_2 + 3\xi}\right) \ . \tag{16}$$

To illustrate the differences between the values of the inertia coefficient as calculated by Eqs. (7–16), in Fig. 2 we show the variation of the inertia coefficient as a function of coordinate ζ for three decay processes of ^{234}U parent nucleus. For the three decay modes, the effective inertia coefficient in the CMAS description is the most reduced one, in contrast with the largest values which are obtained with Werner-Wheeler's inertia coefficient calculated in the VMAS description.

III. COLD FISSION RESULTS

Only ^{234}U parent nucleus exhibits three distinct decay modes: alpha-particle and heavy cluster emissions, and the cold fission process. There are indications that the cold fission

yield of ^{234}U system is about six orders of magnitude lower than its ordinary fission yield (the cold fission half-life for ^{234}U is estimated to order of 10^{30}s [33]).

The challenge for the present model is to continue reproducing the existing data for alpha-particle and heavy-cluster emissions, as well as to reach reasonable prediction for half-life and mass yield distribution for cold fission processes.

In our first work [18] Werner-Wheeler's inertia coefficient and the VMAS description were employed to obtain half-life predictions of alpha decay and heavy cluster emissions from nuclei. The best results for the half-lives were attained by using $r_0 = 1.37\,\mathrm{fm}$. Figure 3 (full line) shows our previous results [18] together with the present ^{234}U cold fission half-life prediction (open diamond). Latter, we proposed an effective inertia coefficient by considering the VMAS description, where the half-lives for alpha decay and cluster emission have been well reproduced with $r_0 = 1.20$ fm [19]. These are shown as dashed line in Fig. 3, together with the present ^{234}U cold fission half-life prediction (open triangle). Next, we extended the CMAS description to calculate cold fission half-lives with Werner-Wheeler's inertia coefficient, but preserving the earlier agreement with the data for alpha decay and cluster radioactivity. We remark that a small change in parameter r_0 was sufficient to attain satisfactory agreement. Dotted lines in Fig. 3 display the results in this case, with $r_0 = 1.31$ fm. The predicted ^{234}U cold fission half-life is represented by open square. The calculation according to the CMAS description, but now using the effective inertia coefficient, is shown as dot-dashed line in Fig. 3. Again, we changed the model parameter in order to obtain the best agreement with the data for alpha decay and cluster radioactivity. By using $r_0 = 1.17$ fm we recalibrated the model for the CMAS description. In this case, the predicted ^{234}U cold fission half-life is represented by open circle.

Table I summarizes the r_0-values which have been used in the calculations to better reproduce the alpha-particle and cluster emission half-lives for the existing data. In Table II we list the predicted cold fission half-life-values for ^{234}U by considering the possible

combinations of descriptions for the pre-scission phase and inertia coefficients, where the r_0 values are those listed in Table I. It is clearly seen that the CMAS description gives the best results for ^{234}U cold fission half-life, independently of the inertia coefficient adopted, when compared with the experimental value.

In order to have an overview of the results obtained with the model when using two different descriptions and inertia coefficients as presented in the precedent Section, we calculated the half-life-values of alpha decay, cluster radioactivity and cold fission processes for all possible parent nuclei where the masses were available from the Mass Table by Audi and Wapstra [31]. The results for the different combinations of inertia coefficients and descriptions for the shape parameterization (see Table I) are displayed in Figs. 4 and 5 for parent mass number $A > 200$. In parts (a) and (b) of Fig. 4 we present the decimal logarithm of the half-life by using, respectively, Werner-Wheeler's and effective inertia coefficients for the VMAS description of the pre-scission phase. In parts (a) and (b) of Fig. 5 we display the decimal logarithm of the half-life when Werner-Wheeler's approximation and effective inertia coefficients are used, respectively, for the CMAS description. Note that when the VMAS description is used throughout the cold fission half-life-values differ significantly from that obtained with Werner-Wheeler's approximation and effective inertia coefficients. Indeed, the results obtained with the effective inertia coefficient are, on the average, ten orders of magnitude higher than those obtained with Werner-Wheeler's inertia coefficients. These results are in complete contrast with those presented in Fig. 5, where the half-life-values for the CMAS description are similar for both inertia coefficients. As a matter of fact, in Fig. 5, where the CMAS description has been used, there is no significant difference between the results when both Werner-Wheeler's and effective inertia coefficients are employed. Figure 5 shows clearly that the CMAS description for the shape parameterization favors the cold fission processes, which are seen as valleys in the upper-right part of the panels. It was already observed in Fig. 3 that the use of the CMAS description is also more appropriate to calculate ^{234}U cold fission half-life data

than the VMAS description for both Werner-Wheeler's and effective inertia coefficients. Note that in all cases the alpha decay and heavy cluster emission processes are rather well reproduced.

Since the CMAS description works well for cold fission using both inertia coefficients, we selected this description to calculate the mass yield distribution for ^{234}U cold fission, and next to compare the results with the extrapolated data for total excitation energy of both fragments TXE $\leq$ 1 MeV by Schwab *et al.* [28]. Results are shown in Fig. 6. The mass-yield distribution comprises more information on the fragmentation process than do the half-life data for a given parent nucleus decay and, therefore, it should be a more strict test for the models. For the partitions obtained with Schwab's extrapolation for ^{234}U cold fission we observe that in the case of the CMAS description our results are in satisfactory agreement with the data, except for the nuclear processes where the mass of the emitted fragment is indicated in the Mass Table as a theoretical prediction using extended mass formula [31]. It is seen Fig. 6 that there is no significant difference between the mass-yield-values, asserting that both inertia coefficients can be equally used to describe the ^{234}U cold fission. All calculations have been performed using the PRESCOLD program [39].

IV. CONCLUSION AND FINAL REMARKS

In the framework of a model which considers two spherical segments for the shape parameterization description, we verified that the model is able to furnish a unified description for alpha decay, cluster radioactivity, and spontaneous cold fission processes for trans-lead nuclei.

We point out that for the two intersecting spheres parameterization to describe the pre-scission phase the potential is defined in the $\{R_1, R_2, \xi, \zeta\}$-manifold, and the two constraints relationships (Eq. (1) and (2)) do restrict the domain of physical interest to a 2-dimensional manifold. Also, the constraint relationships for the VMAS and CMAS de-

scriptions reduce the penetrability calculation to the one-dimensional case. The optimized path for the processes should be determined by the minimization of the action integral in the reduced 2-dimensional manifold, leading to a specific pre-scission description relationship $R_1 = f(\zeta)$, which does not necessarily coincide with that one specified when using the VMAS or CMAS descriptions [20,33]. The actual mass transfer flow through the window connecting the two nascent fragments should be considered as an intermediate situation between the VMAS and CMAS descriptions. The remarkable conclusion is that the CMAS description works satisfactorily in the present model, which is capable to reproduce successfully the existing data for alpha decay, heavy-cluster emission, and cold fission processes in a unified manner.

Although the present stage of the model does not explicitly include fragment deformation in the geometric parameterization, it can be used to obtain a trend for the cold fission processes in which deformed nuclei occurs in the final state. The experimental information about deformation of nuclei is partially included in the Q-value for decay, which is a key element for the effective potential. We remark that the inclusion of deformation in terms of the Q-value for decay is not sufficient to take into account the whole effect of nuclear deformation.

ACKNOWLEDGMENTS

The authors wish to express their gratitude to the Brazilian CNPq and CLAF for partial support.

---

[1] A. Săndulescu and W. Greiner, J. Phys. G **3**, L189 (1977).

[2] A. Săndulescu, H.J. Lustig, J. Hahn, and W. Greiner, J. Phys. G **4**, L279 (1978).

[3] A. Săndulescu, D.N. Poenaru, and W. Greiner, Sov. J. Part. Nucl. **11**, 528 (1980) [Fiz. Elem. Chastits At. Yadra **11**, 1334 (1980)].

[4] H.J. Fink, J. Maruhn, W. Scheid, and W. Greiner, Z. Phys. **268**, 321 (1974).

[5] J. Maruhn and W. Greiner, Phys. Rev. Lett. **32**, 548 (1974).

[6] S.S. Malik, S. Singh, R.K. Puri, S. Kumar, and R.K. Gupta, Pramāna J. Phys. **32**, 419 (1989).

[7] N. Bohr and J.A. Wheeler, Phys. Rev. **56**, 426 (1939).

[8] V.M. Strutinsky, Nucl. Phys. **A95**, 420 (1967).

[9] V. Avrigeanu, A. Florescu, A. Săndulescu, and W. Greiner, Phys. Rev. C **52**, R1755 (1995).

[10] J. H. Hamilton, A.V. Ramayya, J. Kormicki, W.-C. Ma, Q. Lu, D. Shi, J.K. Deng, S.J. Zhu, A. Săndulescu, W. Greiner, G.M. Ter-Akopian, Yu. Ts. Oganessian, G.S. Popeko, A.V. Daniel, J. Kliman, V. Polhorsky, M. Morhac, J.D. Cole, R. Aryaeinejad, I.Y. Lee, N.R. Johnson, and F.K. McGowan, J. Phys. G **20**, L85 (1994); J.H. Hamilton, A.V. Ramayya, S.J. Zhu, G.M. Ter-Akopian, Yu. Ts. Oganessian, J.D. Cole, J.O. Rasmussen, and M.A. Stoyer, Prog. Part. Nucl. Phys. **35**, 635 (1995).

[11] A. Benoufella, G. Barreau, M. Asghar, P. Audouard, F. Brisard, T.P. Doan, M. Hussonnois, B. Leroux, J. Trochon, and M.S. Moore, Nucl. Phys. A**565**, 563 (1993).

[12] A. Săndulescu, A. Florescu, F. Carstoiu, and W. Greiner, J. Phys. G **22**, L87 (1996).

[13] E. Stefanescu, W. Scheid, A. Săndulescu, and W. Greiner, Phys. Rev. C **53**, 3014 (1996).

[14] A. Săndulescu, A. Florescu, F. Carstoiu, W. Greiner, J.H. Hamilton, A.V. Ramayya, and B.R.S. Babu, Phys. Rev. C **54**, 258 (1996).

[15] A. Florescu, A. Săndulescu, C. Cioaca, and W. Greiner, J. Phys. G **19**, 669 (1993).

[16] A. Florescu, A. Săndulescu, and W. Greiner, J. Phys. G **19**, 1947 (1993).

[17] S. Singh, R.K. Gupta, W. Scheid, and W. Greiner, J. Phys. G **18**, 1243 (1992).

[18] M. Gonçalves and S.B. Duarte, Phys. Rev C **48**, 2409 (1993).

[19] S.B. Duarte and M.G. Gonçalves, Phys. Rev. C **53**, 2309 (1996).

[20] R.A. Gherghescu, W. Greiner, and D. N. Poenaru, Phys. Rev. C **52**, 2636 (1995).

[21] E. Stefanescu, A. Săndulescu, and W. Greiner, J. Phys. G **20**, 811 (1994).

[22] D.N. Poenaru and W. Greiner, J. Phys. G **17**, S443 (1991).

[23] W. Greiner and A. Săndulescu, J. Phys G **17**, S429 (1991).

[24] W. Mollenkopf, J. Kaufmann, F. Gönnenwein, P. Geltenbort, and A. Oed, J. Phys. G **18**, L203 (1992).

[25] H.-H. Knitter, F.-J. Hambsch, and C. Budtz-Jørgensen, Nucl. Phys. A**536**, 221 (1992).

[26] G.M. Ter-Akopian, J.M. Hamilton, Yu. Ts. Oganessian, J. Kormicki, G.S. Popeko, A.V. Daniel, A.V. Ramayya, Q. Lu, K. Butler-Moore, W.-C. Ma, J.K. Deng, D. Shi, J. Kliman, V. Polhorsky, M. Morhac, W. Greiner, A. Săndulescu, J.D. Cole, R. Aryaeinejad, N.R. Johnson, I.Y. Lee, and F.K. McGowan, Phys. Rev. Lett. **73**, 1477 (1994).

[27] M. Asghar, N. Boucheneb, G. Medkour, P. Geltenbort, and B. Leroux, Nucl. Phys. A**560**, 677 (1993).

[28] W. Schwab, H.-G. Clerc, M. Mutterer, J.P. Theobald, and H. Faust, Nucl. Phys. A**577**, 674(1994).

[29] Y.X. Dardenne, R. Aryaeinejad, S.J. Azstalos, B.R.S. Babu, K. Butler-Moore, S.Y. Chu, J.D. Cole, M.W. Drigert, K.E. Gregorich, J.H. Hamilton, J. Kormicki, I.Y. Lee, R.W. Lougheed, Q.H. Lu, W.-C. Ma, M.F. Mohar, K.J. Moody, S.G. Prussin, A.V. Ramayya, J.O. Rasmussen, M.A. Stoyer, and J.F. Wild, Phys. Rev. C **54**, 206 (1996).

[30] L. Demattè, C. Wagemans, R. Barthélémy, P. D'hondt, and A. Deruytter, Nucl. Phys.

A**617**, 331 (1997).

[31] G. Audi and A.H. Wapstra, Nucl. Phys. A**595**, 409 (1995).

[32] D.N. Poenaru, W. Greiner, and E. Hourani, Phys. Rev. C **51**, 594 (1995).

[33] M. Mirea, D.N. Poenaru, and W. Greiner, Z. Phys. A **349**, 39 (1994).

[34] M. Mirea, D.N. Poenaru, and W. Greiner, Z. Phys. A **349**, 39 (1994); Nuovo Cimento A**105**, 571 (1992).

[35] G. A. Pik-Pichak, Sov. J. Nucl. Phys. **44**, 923 (1986) [Yad. Fiz. **44**, 1421 (1986)].

[36] D.N. Poenaru, J.A. Maruhn, W. Greiner, M. Ivascu, D. Mazilu, and I. Ivascu, Z. Phys. A **333**, 291 (1989).

[37] G. Gamow, Z. Phys. **51**, 204 (1928).

[38] G. Shanmugam, G.M. Carmel Vigila Bai, and B. Kamalaharam, Phys. Rev. C **51**, 2616 (1995).

[39] M. Gonçalves, S.B. Duarte, F. García and O. Rodriguez, Comp. Phys. Comm. **107** (1997) 246.

V. TABLE CAPTIONS

TABLE I: Values of r_0 which give the best agreement of calculated with experimental half-life-values for alpha decay and cluster radioactivity of heavy parent nuclei (cf. Fig. 3).

TABLE II: Predicted cold fission half-life-values for ^{234}U parent nucleus as obtained with the r_0-values listed in Table I.

TABLES:

TABLE I:

Description of shape parameterization	r_0-values (in fm) Werner-Wheeler's approximation (μ_{WW})	Effective inertia (μ_{eff})
Varying mass asymmetry shape (VMAS)	1.37	1.20
Constant mass asymmetry shape (CMAS)	1.31	1.17

TABLE II

Description of shape parameterization	$\log_{10}\tau$, τ in second* Werner-Wheeler's approximation (μ_{WW})	Effective inertia (μ_{eff})
VMAS	21.81	39.31
CMAS	28.92	31.32

*Experimental half-life-value: $\log_{10}\tau = 30$ (see Ref. [33]).

FIGURE CAPTIONS

Fig. 1: Potential barrier height in the VMAS (full line) and CMAS (dashed line) descriptions for alpha emission (a), cluster radioactivity (b), and spontaneous cold fission process (c) of ^{234}U parent nucleus.

Fig. 2: Inertia coefficient, μ, plotted against separation between the centers of the nascent fragments, ζ, for three modes of decay of ^{234}U parent nucleus. In Werner-Wheeler's approximation the μ-values in the VMAS description ($\mu_{\rm WW}^{\rm VMAS}$) are represented by full lines, while the ones in the CMAS description ($\mu_{\rm WW}^{\rm CMAS}$) by dot-dashed lines; the values of effective inertia coefficient in the VMAS description ($\mu_{\rm eff}^{\rm VMAS}$) are shown by dashed lines, while in the CMAS description ($\mu_{\rm eff}^{\rm CMAS}$) by dotted lines.

Fig. 3: Calculated half-life values as obtained by the different descriptions for the shape parameterization and inertia coefficients as indicated in a). Part a) displays the results for cluster radioactivity together with cold fission of ^{234}U; in b) we present the results for alpha decay. Experimental data are represented by filled symbols.

Fig. 4: Contour plot of the decimal logarithm of the fragment-decay half-life calculated in the VMAS description using Werner-Wheeler's approximation (a) and effective inertia (b) coefficients. All cases for which the mass-values (A $>$ 200) were available from the most recent Mass Table [31] have been considered. Half-life-ranges are indicated by the color $\log_{10}$-scale.

Fig. 5: The same as in Fig. 4 for the CMAS description of the pre-scission phase.

Fig. 6: Calculated mass-yield distribution for ^{234}U cold fission in the CMAS description of the pre-scission phase with Werner-Wheeler's approximation (a) and effective inertia (b) coefficients (open squares connected by dotted line). Extrapolated data for total excitation energy of both fragments TXE $\leq$ 1 MeV taken from Ref. [28] are represented by filled circles.

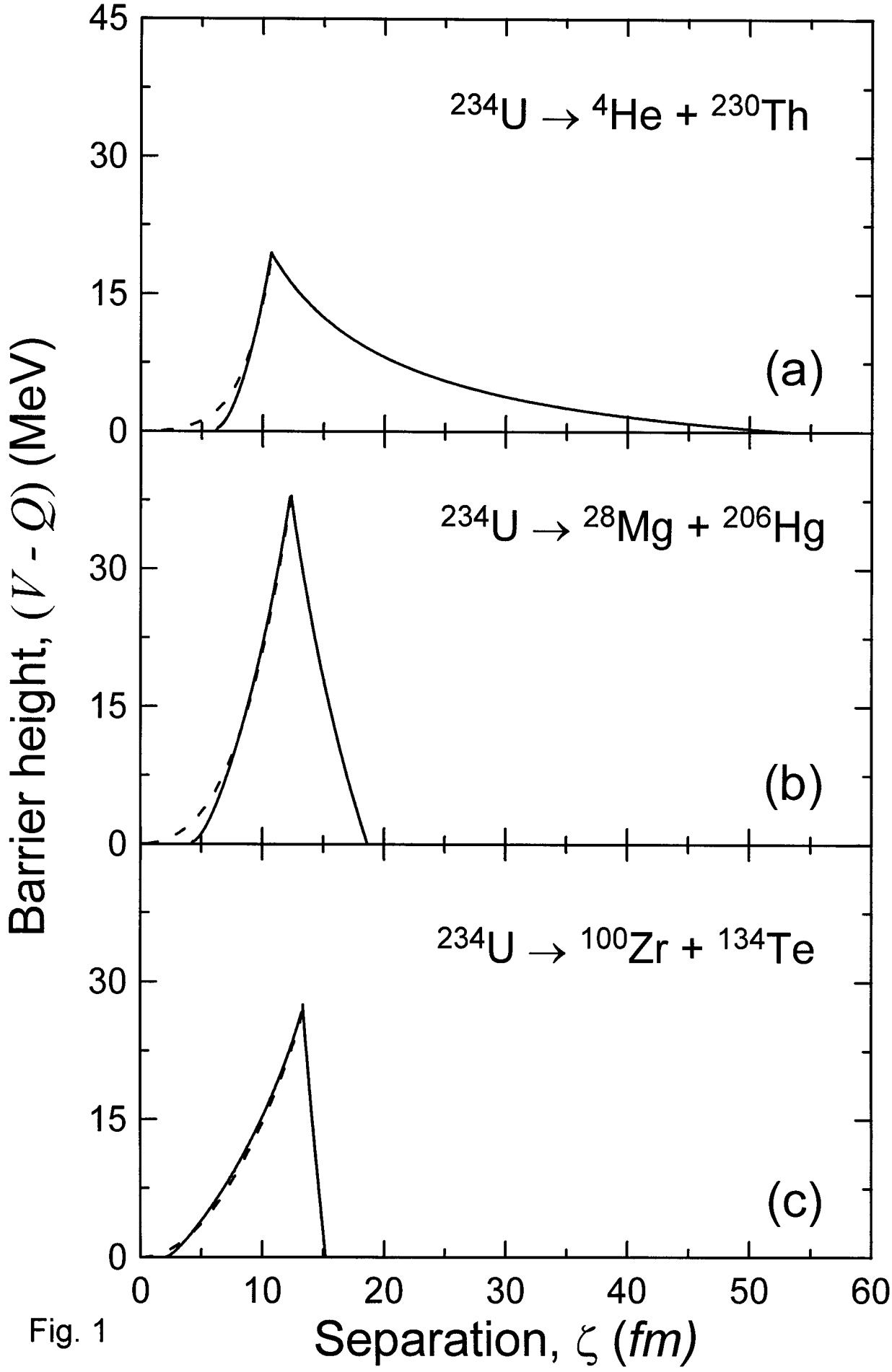
$^{234}U \rightarrow {}^{4}He + {}^{230}Th$
(a)
$^{234}U \rightarrow {}^{28}Mg + {}^{206}Hg$
(b)
$^{234}U \rightarrow {}^{100}Zr + {}^{134}Te$
(c)
Barrier height, $(V - Q)$ (MeV)
Separation, ζ (*fm*)
0
15
30
45
0
10
20
30
40
50
60

Fig. 1

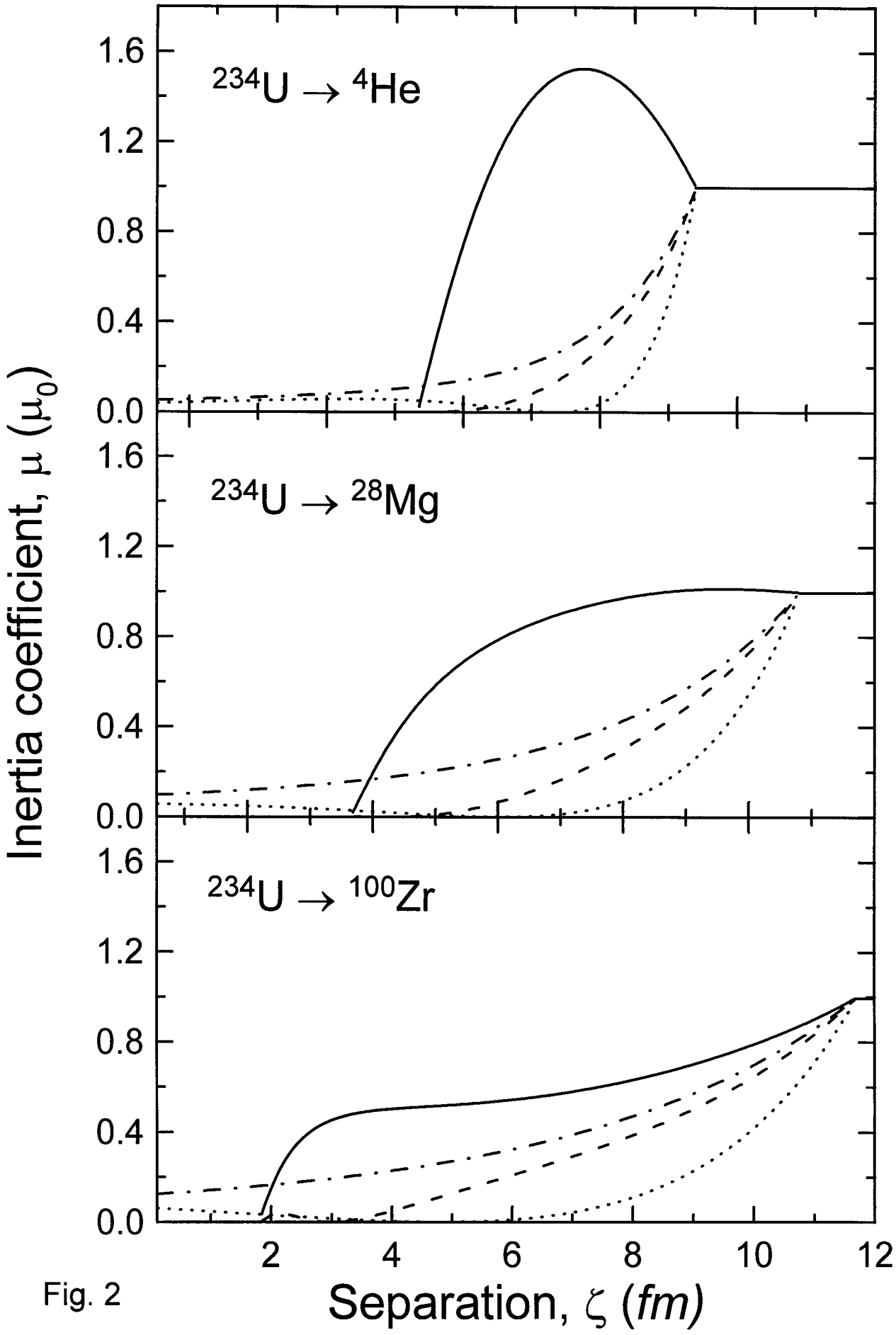
$^{234}U \rightarrow {}^{4}He$
$^{234}U \rightarrow {}^{28}Mg$
$^{234}U \rightarrow {}^{100}Zr$
Inertia coefficient, μ (μ_0)
Separation, ζ (*fm*)
0.0
0.4
0.8
1.2
1.6
2
4
6
8
10
12

Fig. 2

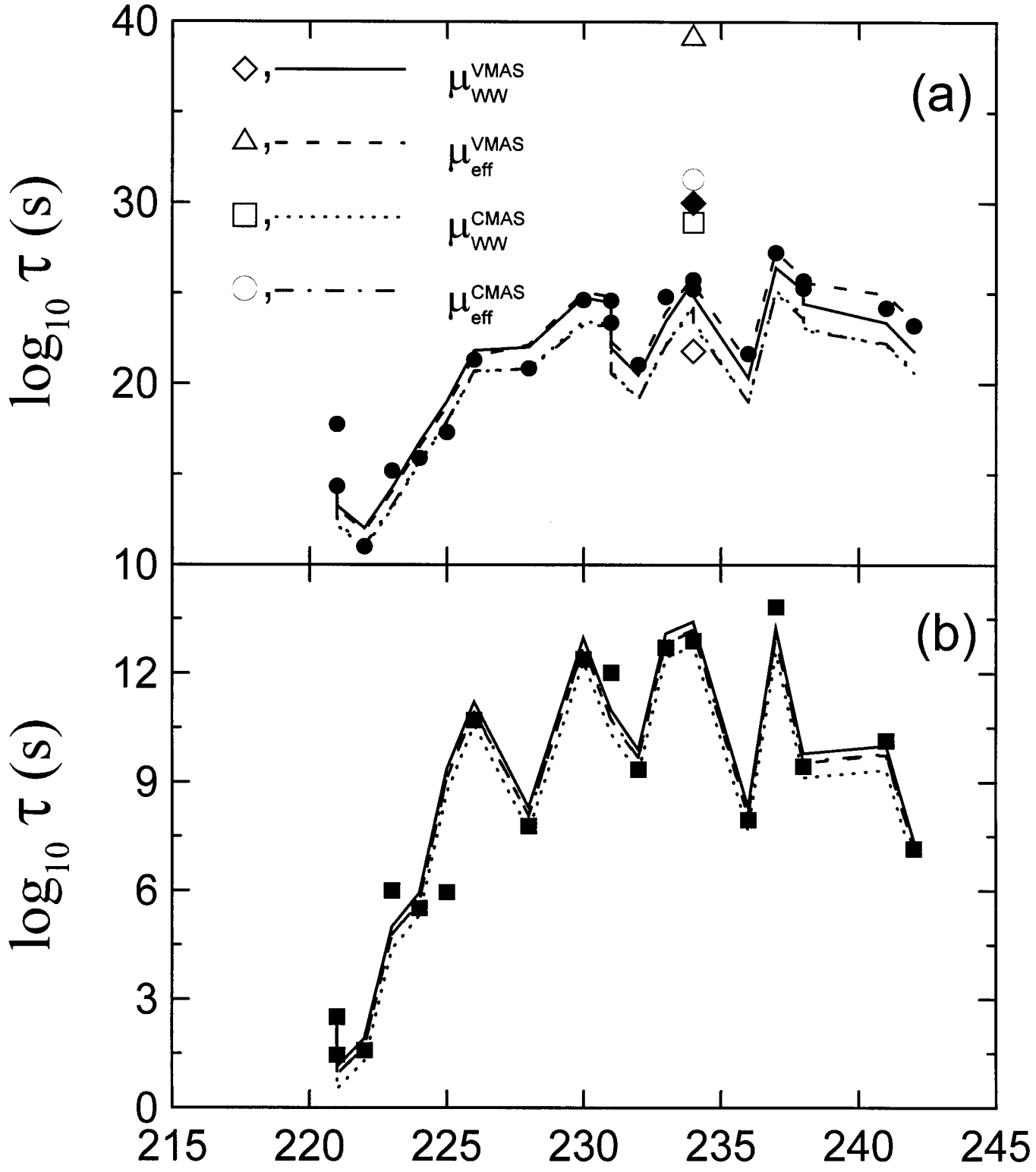
40
30
20
10
$\log_{10}\tau$ (s)
μ^{VMAS}_{WW}
μ^{VMAS}_{eff}
μ^{CMAS}_{WW}
μ^{CMAS}_{eff}
(a)
(b)
12
9
6
3
0
215
220
225
230
235
240
245
Parent nucleus mass number

Fig. 3

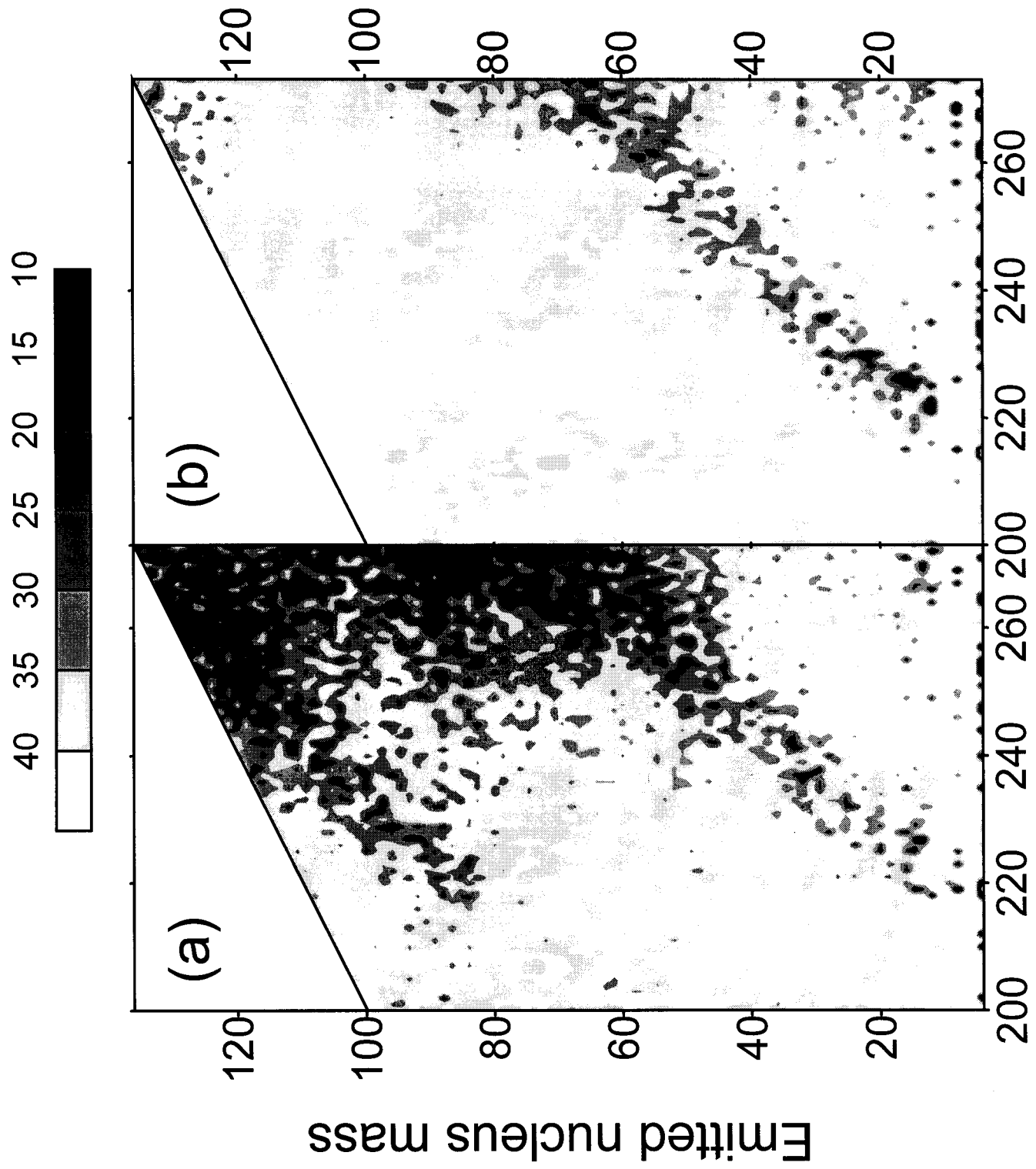
40 35 30 25 20 15 10
(a)
(b)
120 100 80 60 40 20
200 220 240 260
Emitted nucleus mass
Parent nucleus mass

Fig. 4

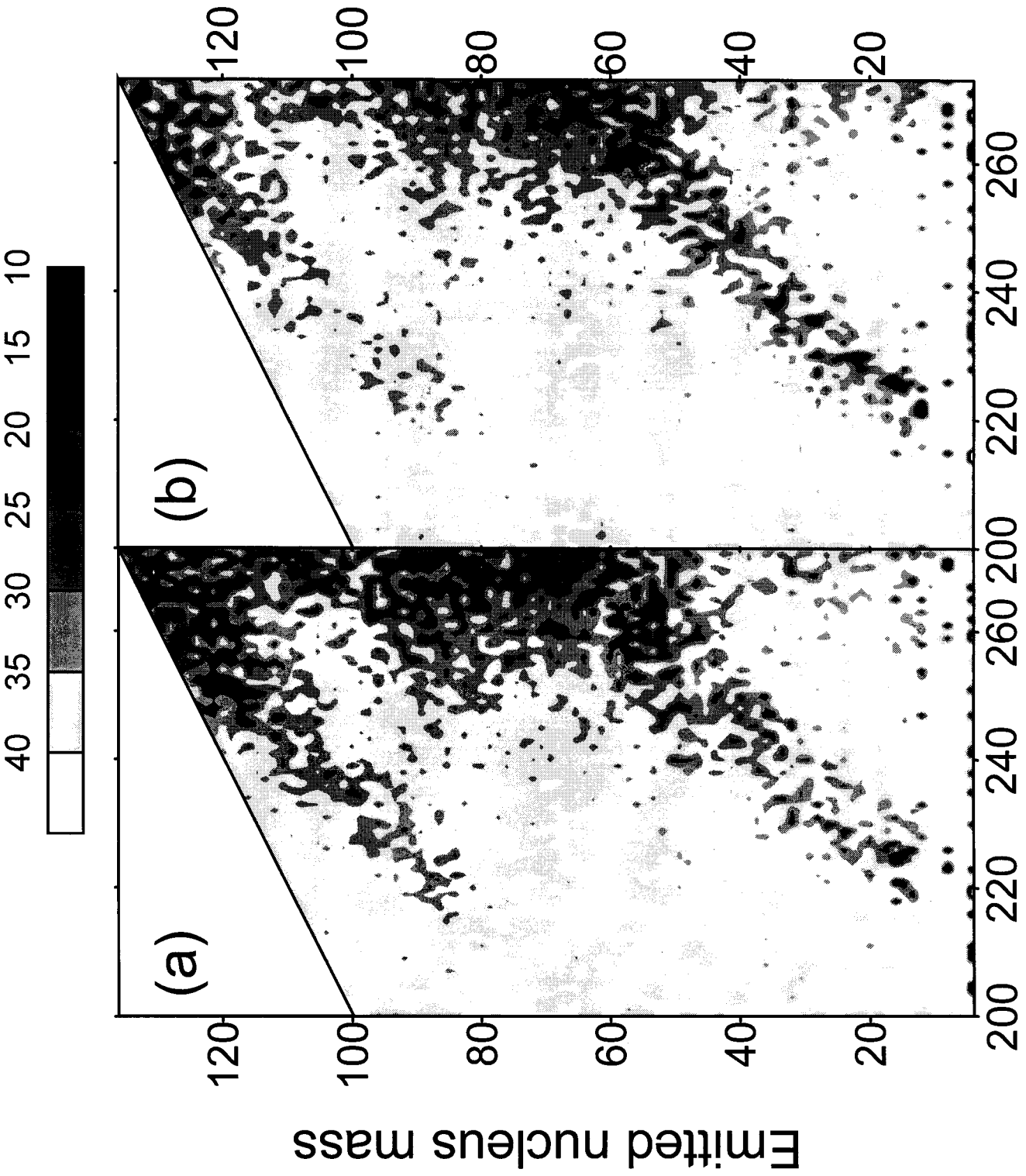
(a)
(b)
Emitted nucleus mass
Parent nucleus mass
120
100
80
60
40
20
200
220
240
260
40 35 30 25 20 15 10

Fig. 5

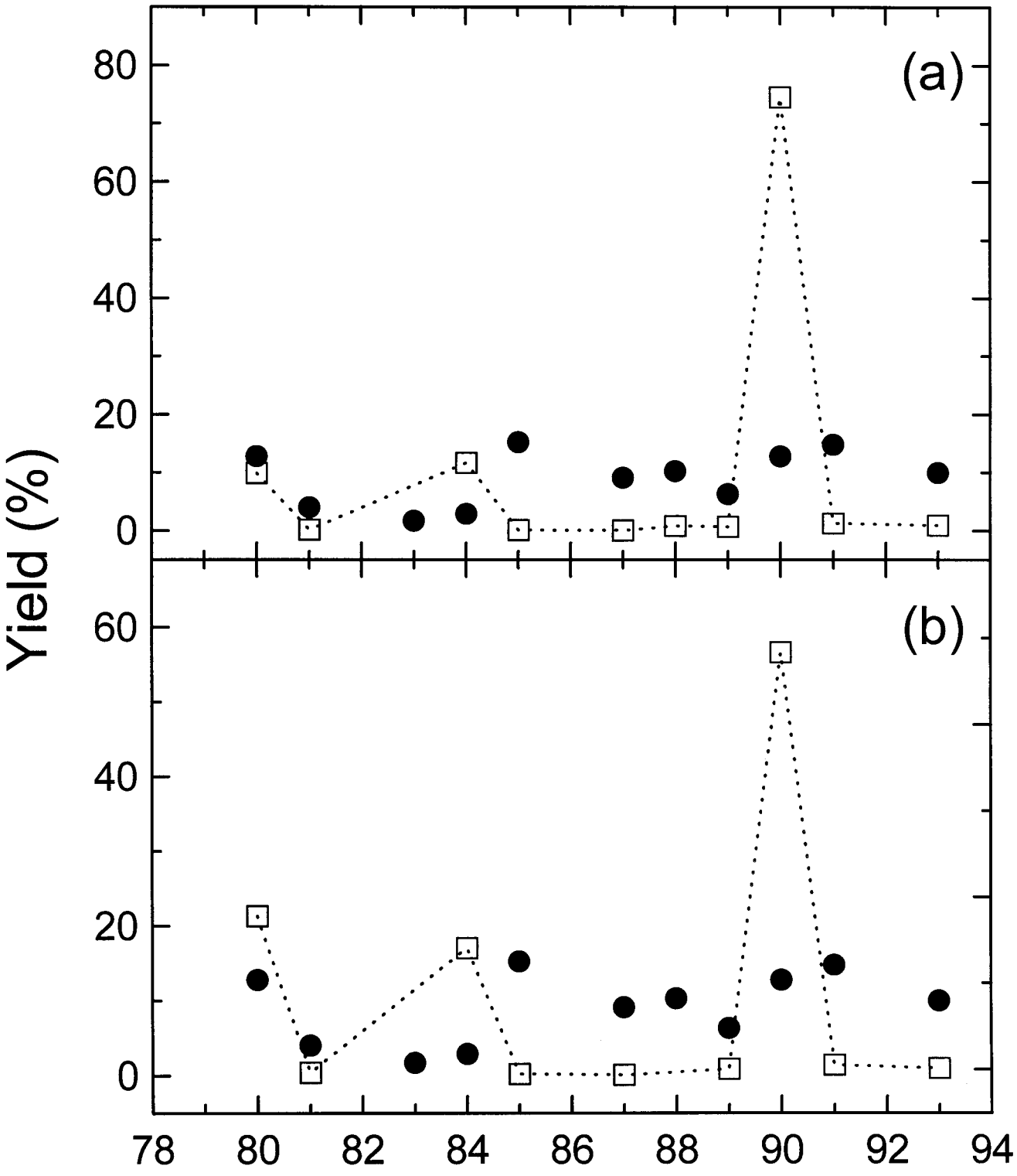
(a)
(b)
Yield (%)
80
60
40
20
0
60
40
20
0
78
80
82
84
86
88
90
92
94
Light fragment mass number, A_L

Fig. 6